

Diatomic Line Strengths for Fitting Selected Molecular Transitions of AlO, C₂, CN, OH, N₂⁺, NO, and TiO, Spectra

Christian G. Parigger 

Physics and Astronomy Department, University of Tennessee, University of Tennessee Space Institute, Center for Laser Applications, 411 B.H. Goethert Parkway, Tullahoma, TN 37388-9700, USA; cparigge@tennessee.edu; Tel.: +1-(931)-841-5690

Abstract: This work communicates line-strength data and associated scripts for the computation and spectroscopic fitting of selected transitions of diatomic molecules. The scripts for data analysis are designed for inclusion in various software packages or program languages. Selected results demonstrate the applicability of the program for data analysis in laser-induced optical breakdown spectroscopy primarily at the University of Tennessee Space Institute, Center for Laser Applications. Representative spectra are calculated and referenced to measured data records. Comparisons of experiment data with predictions from other tabulated diatomic molecular databases confirm the accuracy of the communicated line-strength data.

Keywords: diatomic molecules; laser-plasma; data analysis; laser-induced breakdown spectroscopy; combustion; spectroscopy, spectra-fitting program; astrophysics

1. Introduction

Atomic, molecular, optical (AMO) spectroscopy furnishes fundamental insight by decoding light emanating from targets of interest [1–8]. Analytical studies of elements may be straightforward, especially for elements that appear in the first three rows of the period table. Balmer-series hydrogen lines or sodium D-lines usually are well separated from spectral interference for low (~1 eV)-temperature plasma containing sodium as long as reasonable resolving power is available. For example, for the sodium D-lines, a resolving power, R , of $R \simeq 1000$ is needed to distinguish the two components D1 and D2, separated by ~0.06 nm. Resolving individual lines of molecular spectra may require $R > 10,000$, or at least of the order of one magnitude better resolution than needed for atoms, of course depending on temperature. In molecular spectroscopy, one tends to focus on molecular bands describing electronic transitions. The study of individual atomic or molecular resonances with continuous-wave radiation typically requires GHz scans with nominal MHz or better laser bandwidths. In this work, the focus is on optical spectrometers that measure near-UV to near-IR molecular bands with a spectral resolution, $\delta\lambda$, of the order of $\delta\lambda \sim 0.1$ nm.

A collection of molecular diatomic spectroscopy data and expansive literature review and guidance [9] reveals a volley of recent and updated records in the UV to IR wavelength range. However, this work's focus is the visible and near-IR, specific sets of electronic transition data that have been tested in the analysis of experimental records. The mentioned databases [9] predict OH spectra among many others for diatomic molecules, e.g., ExoMol [10] and HITEMP [11] that can be visualized using for example PGOPHER [12]—PGOPHER also allows one to model transitions for prediction and comparative analysis. Selected diatomic molecular spectra of AlO, C₂, CN, OH, N₂⁺, NO, and TiO, transitions are of interest as these can be observed in laser-induced breakdown spectroscopy (LIBS) [13–15] at standard ambient temperature and pressure (SATP). Diatomic AlO and TiO spectra usually occur following the creation of micro-plasma near or at aluminum and titanium surfaces, respectively. In several cases, molecular spectra may not be of primary interest in elemental



Citation: Parigger, C.G. Diatomic Line Strengths for Fitting Selected Molecular Transitions of AlO, C₂, CN, OH, N₂⁺, NO, and TiO, Spectra. *Foundations* **2023**, *3*, 1–15. <https://doi.org/10.3390/foundations3010001>

Academic Editor: Cristina Achim

Received: 25 October 2022

Revised: 29 November 2022

Accepted: 23 December 2022

Published: 1 January 2023



Copyright: © 2023 by the author. Licensee MDPI, Basel, Switzerland. This article is an open access article distributed under the terms and conditions of the Creative Commons Attribution (CC BY) license (<https://creativecommons.org/licenses/by/4.0/>).

analysis with LIBS using nanosecond laser pulses, but molecular spectra are readily observed with femtosecond laser-plasma excitation, or after some time delay (of the order of larger than 100 ns for occurrence of CN in CO₂:N₂ gas mixtures) from optical breakdown when using nanosecond laser pulses. Just as for atomic spectra, reasonably accurate molecular spectra are required for analysis [16–20]. The construction of a molecular spectrum relies on: (i) accurate line positions, and (ii) reasonably accurate transition strengths [21–24]. For the former, numerical singular value decomposition is employed for upper and lower states of a particular transition. For the latter, Frank–Condon factors and r-centroids are computed, and then combined with the rotational factors that usually decouple from the overall molecular line strength due to the symmetry of diatomic molecules.

This work communicates data files and associated scripts for the computation of diatomic molecular spectra, and equally, for the fitting of measured data using a nonlinear fitting algorithm. Calculated spectra are presented and references to recorded datasets are provided. Applications comprise fields of chemistry, materials science, astronomy, and finally physics including astrophysics, e.g., decoding of light from white dwarf stars such as Procyon B. The data are provided as a set of wave numbers, upper-level term value, and line strength. Originally, FORTRAN/Windows 7 programs computed diatomic molecular spectra [21], but the scripts for the generation of molecular spectra are redesigned for use with MATLAB [25]. Moreover, this work communicates MATLAB-optimized line-strength files (LSFs) containing three columns, namely wave numbers, upper term values, and line strengths. The codes are operating system-independent as long as MATLAB or similar programs are available that allow scripts similar to the ones available in MATLAB. Supplementary data contain programs and nine selected diatomic molecular transitions of AlO, C₂ Swan, CN red, CN violet, OH ultraviolet, N₂⁺, NO gamma, TiO γ, and TiO γ'.

2. Materials and Methods

The computation of diatomic molecular spectra uses established line-strength data. Programs in FORTRAN accomplish the generation of spectra, coupled with a separate plotting program for visualization, including convenient implementation using a Microsoft-Windows 7 operating system. This work communicates equivalent MATLAB scripts that appear popular with various research groups. First, the Boltzmann equilibrium spectral program (BESP) generates a theoretical spectrum, and second, the Nelder–Mead temperature (NMT) program accomplishes fitting of experimental and theoretical spectra. In principle, BESP can be used to generate maps as a function of temperature and linewidth with subsequent determination of the optimum solution with minimal errors in the least-square sense. In turn, NMT uses nonlinear optimization using geometric constructs, viz. simplices. The accumulation of experimental spectra in this work is in accord with laser-induced breakdown spectroscopy, or in general, laser spectroscopy [26].

2.1. MATLAB Scripts

The parameter list includes wavelength minimum, maximum, temperature, number of points, normalization factor, and file name. For the BESP.m and NMT.m scripts, the outputs are generated in graphical form. Table 1 lists constants that could be used (comment line in the scripts) for the determination of the variation of the refractive index, *n*, of air with wavelength [27],

$$10^6(n - 1) = a_0 + \frac{a_1}{\lambda_N^2} + \frac{a_2}{\lambda_N^4}, \quad (1)$$

where λ_N is the wavelength in normal air at 15 °C and 101,325 Pa (760 mm Hg), expressed in terms of micrometer (range 0.2218–0.9000 μm).

Table 1. Constants for variation of refractive index, n ; see Equation (1).

Parameter	Value
a_0	272.643
a_1	1.2288 (μm^2)
a_2	0.03555 (μm^4)

Table 2 lists constants that are used to account for the variation of the refractive index, r_i , of air at 15 °C, 101,325 Pa, and 0% humidity, with wavenumber [28],

$$10^8(r_i - 1) = \frac{k_1}{(k_0 - \sigma^2)} + \frac{k_3}{(k_2 - \sigma^2)}, \quad (2)$$

where σ is the wavenumber in units of μm^{-1} .

Table 2. Constants for variation of refractive index; see Equation (2).

Parameter	Value (μm^{-2})
k_0 (k0)	238.0185
k_1 (k1)	5,792,105
k_2 (k2)	57.362
k_3 (k3)	167,917

Tables 3 and 4 summarize script constants and input variables that are important for spectra computations, respectively. However, redesign of BESP.m and NMT.m from the FORTRAN/Windows 7 version [21] was accomplished with extensive discussions [24]. Edited versions of BESP.m and NMT.m are communicated in this work along with nine separate data files.

Table 3. Constants in BESP.m and NMT.m.

Constant	Value
Planck constant (h)	$6.62606957 \times 10^{-34}$ (J s)
speed of light (c)	2.99792458×10^8 (m s $^{-1}$)
Boltzmann constant (kb)	$1.3806488 \times 10^{-23}$ (J K $^{-1}$)

Table 4. Parameters and variables in BESP.m and NMT.m.

Description	Variable
wavelength minimum	wl_min (cm $^{-1}$)
wavelength maximum	wl_max (cm $^{-1}$)
temperature	T (kK)
full-width at half maximum	FWHM, $\delta\lambda$ (nm)
number of points	N
normalization	norm
file name	x

2.1.1. BESP.m

The script BESP.m is designed following the FORTRAN/Windows 7 version [21]. The individual diatomic molecular data files for selected transitions are concatenated to only show wavenumbers, upper-term values, and line strengths; see Table 5. Adjustments of input parameters for MATLAB [25] are rather straightforward, equally, for generalizing the script for automatic input by converting the script to a function. Individual lines are computed using Gaussian profiles [21], and for the generation of a spectrum, only one temperature is needed for equilibrium computation. Conversely, as one infers temperature

from a measured spectrum, a modified Boltzmann plot [22] is constructed for the determination of the equilibrium temperature. A Gaussian line shape is selected to model the spectrometer/intensifier transfer function profile. However, one usually considers a natural linewidth for electronic state-to-state transitions, and a Gaussian line shape for Doppler broadening [29], viz.

$$\Delta\lambda = 7.16 \times 10^{-7} \lambda \sqrt{\frac{T}{M}}, \quad (3)$$

leading to Voigt line shapes. Here, $\Delta\lambda$ is the full-width half-maximum, λ the wavelength, T the temperature, and M the molecular weight. For example, with $\lambda = 306$ nm, $T = 3.5$ kK, and $M = 17$ (OH), $\Delta\lambda = 0.0031$ nm. The spectral resolution, $\delta\lambda$, for the OH emission spectral-fitting, discussed in the Appendix, amounts to $\delta\lambda = 0.33$ nm. Consequently, a Gaussian line shape is considered instead of a Voigt line shape for fitting of the OH data in the appendix, but the communicated MATLAB scripts can be adjusted for Voigt profiles, important for cases when individual electronic state-to-state molecular transitions/resonances are investigated. Equally, when investigating individual transitions/resonances, asymmetric molecular line shapes can be implemented in the scripts. There is usually a volley of lines for electronic transitions of a diatomic molecules, e.g., OH [30] in excess of 3 kK, within a wavelength bin and for an experimental spectral resolution of the order of 0.33 nm.

The program BESP.m receives input from the LSFs that contain relative line strengths. The output is generated in graphical format, and the program is slightly adjusted for the generation of the spectra illustrated in Figures 1–9. However, Figure 6 is generated with the BESP.m script given below.

```
% BESP.m
%
% Calculates diatomic spectra using line strength data files constructed for selected transitions.
% The program is designed using a previous FORTRAN/Windows7 implementation including private communications
% with James O. Hornkohl and David M Surmick.
%
% David M. Surmick, 04–27–2016; edited by Christian G. Parigger 11–27–2022.

% input parameters, output: WL_exp (N–1 x 1 array), I (intensity)
wL_min=300; wL_max=325; T=3530; FWHM=0.35; N=10001; norm=1; x='OH-lsf.txt';

% generate wavelengths/wavelength-bins for computation akin to an experiment
nSpec=N–1; delWL=(wL_max–wL_min)/(nSpec); WL_exp=linspace(wL_min,wL_max,nSpec); WL_exp=WL_exp';

% constants in MKS units (Boltzmann factor bFac in cgs units)
h=6.62606957e–34; c=2.99792458e8; kb=1.3806488e–23; bFac=(100*h*c)/kb; gFac=2*sqrt(log(2));

% read line strength file
[p]=load(x); WN=p(:,1); Tu=p(:,2); S=p(:,3);

% convert vacuum wavenumber to air wavelength: CGP 11–27–2022
%a0=2.72643e–4; a1=1.2288; a2=3.555e4; r=1+a0+(a1./(WN.*WN))+(a2./(WN.*WN.*WN.*WN));
k0=238.0185; k1=5792105; k2=57.362; k3=167917; r=(1+k1./(1d8*k0–(WN.*WN)))+k3./(1d8*k2–(WN.*WN)); WL=1.e7./(r.*WN);

% get LSF table wavelengths that most closely match the wavelength-bins
A=find(WL>wL_min & WL<wL_max); WLk=WL(A);

% get term values and line strengths at WLk in the range wL_min to wL_max
Sk=S(A); Tuk=Tu(A); TuMin=min(Tuk);

% calculate peak intensities and initialize peak_k calculation
peak=–4*log(WLk)+log(Sk)–(bFac/T)*(Tuk–TuMin); peak_k=zeros(nSpec,1); peakMax=–1;
for i=1:length(peak);
    if peak(i) > peakMax; peakMax=peak(i); end;
    if peak(i) ~= 0; peak_k(i)=peak(i)–peakMax; end;
end; peak_k=exp(peak_k);

% get wavelength-bin positions that most closely matches line strength table wavelengths
n0=zeros(length(WLk),1); for i=1:length(WLk); [~,n0(i)]=min(abs(WL_exp–WLk(i))); end;

% calculate spectrum using Gaussian profiles for peaks, and for wavelength dependent FWHM
I=zeros(nSpec,1); FWHMk=(FWHM*WLk)/wL_max;
```

```

for i=1:length(WLk); deln=round(FWHM/delWL,0); nMin=n0(i)-deln;
if nMin < 1; nMin=1; end; nMax=n0(i)+deln;
if nMax > nSpec; nMax=nSpec; end;
for j=nMin:nMax; u=abs(gFac*(WL_exp(j)-WLk(i))/FWHMk(i));
if u <=9.21; I(j)=I(j)+peak_k(i)*exp(-u*u); end;
end;
end; I=norm*I/max(I);

%Display graphical output
figure; plot(WL_exp,I,'LineWidth',1.5); set(gca,'FontWeight','bold','FontSize',20,'TickLength',[0.02, 0.02]);
LimitsX=xlim; LimitsY=ylim; title(' ','HorizontalAlignment','left','Position',[LimitsX(1)-4,LimitsY(2)]);
xlabel('wavelength (nm)','FontSize',24,'FontWeight','bold');
ylabel('intensity (a.u.)','FontSize',24,'FontWeight','bold');

```

2.1.2. NMT.m

The NMT script details are deferred to Appendix A. The adaptation of a previous FORTRAN code with Windows 7 libraries for a Microsoft platform is no longer viable due to support discontinuation of the Windows 7 operating system. However, the NMT.m script delivers spectra-fitting results identical to those obtained with the FORTRAN/Windows 7 implementation.

2.1.3. Data Files

This section explains the line-strength data communicated in this work. The line-strength files (LSFs) contain wave numbers, upper term values, and the line strengths. Table 5 summarizes contents of line-strength data. The air wavelength in the program, WL, is in units of nm. The two programs BESP and NMT convert the vacuum wave numbers to air wavelengths for the analysis of measured data; see Equation (1). Table 6 associates the diatomic molecules and their line-strength data, including the wavelength range.

The LSFs contain significantly more data than illustrated in this communication. Applications of the LSFs include data analysis of laser-induced fluorescence and computation of absorption spectra. Some of these applications are elaborated on in the discussion of C₂ Swan spectra [23].

Table 5. Line-strength data contents: Vacuum wave numbers and upper term values, line strengths.

Description	Variable	Column
wave number	WN (cm ⁻¹)	1
upper term value	Tu (cm ⁻¹)	2
line strength	S (stC ² cm ²) ^a	3

^a 1 stC = 3.356 10⁻¹⁰ C.

Table 6. Diatomic molecules, line-strength data files, wavelength range, and number of spectral lines.

Diatomic Molecule	Line-Strength Data File	Wavelength Range (nm)	Number of Spectral Lines
aluminum monoxide (AlO)	AlO-BX-LSF.txt	430.72–997.66	33,484
carbon Swan spectra (C ₂)	C2-Swan-LSF.txt	410.93–678.58	29,004
cyanide red (CNr) system	CNr-LSF.txt	499.89–4997.56	40,728
cyanide violet (CNv) system	CNv-LSF.txt	372.88–425.22	7960
hydroxyl (OH) violet system	OH-LSF.txt	278.65–379.72	1683
nitrogen monoxide (NO) gamma system	NO-GAMMA-LSF.txt	200.41–285.95	13,000
singly ionized nitrogen (N ₂ ⁺)	N2p-LSF.txt	319.04–501.46	7302
titanium monoxide (TiO) γ band	TiO-AX-LSF.txt	599.58–945.44	66,962
titanium monoxide (TiO) γ' band	TiO-BX-LSF.txt	582.73–679.12	34,648

3. Results

This section summarizes the communicated line-strength data. Table 7 associates the diatomic molecules and their line-strength files (LSF). The LSFs contain wave numbers, upper term values and the line strength. The two programs BESP and NMT convert the vacuum wave numbers to air wavelengths for the analysis of measured data. Table 7 displays spectral resolution, temperature, and Table 7 also communicates but one reference each for measurement and fitting selected molecular transitions of AlO, C₂, CN, OH, N₂⁺, NO, and TiO. Figures 1–9 illustrate computed spectra that refer to measured ones in the references.

Table 7. Diatomic molecules, spectral resolution, temperature, and one typical reference each that uses the data.

Diatomic Molecule	Line-Strength Data	Spectral Resolution (nm)	Temperature (kK)	Reference	Figure
aluminum monoxide (AlO)	AlO-BX-LSF.txt	1.0	3.33	[31]	Figure 1
carbon Swan spectra (C ₂)	C2-Swan-LSF.txt	0.39	6.75	[32]	Figure 2
cyanide red (CNr) system	CNr-LSF.txt	0.38	7.5	[33] ^a	Figure 3
cyanide violet (CNv) system	CNv-LSF.txt	0.030	7.94	[34]	Figure 4
singly ionized nitrogen (N ₂ ⁺)	N2p-LSF.txt	0.035	5.1	[35]	Figure 5
hydroxyl (OH) ultraviolet system	OH-LSF.txt	0.35	3.39	[30]	Figure 6
nitrogen monoxide (NO) gamma system	NO-GAMMA-LSF.txt	0.056	6.8	[36]	Figure 7
titanium monoxide (TiO) γ band	TiO-AX-LSF.txt	0.10	3.03	[37] ^b	Figure 8
titanium monoxide (TiO) γ' band	TiO-BX-LSF.txt	0.40	3.6	[38]	Figure 9

^a Experiments at Johannes Kepler University, Linz, Austria. ^b Experiments in part at Chemical Research Center of the Hungarian Academy of Science, Budapest, Hungary.

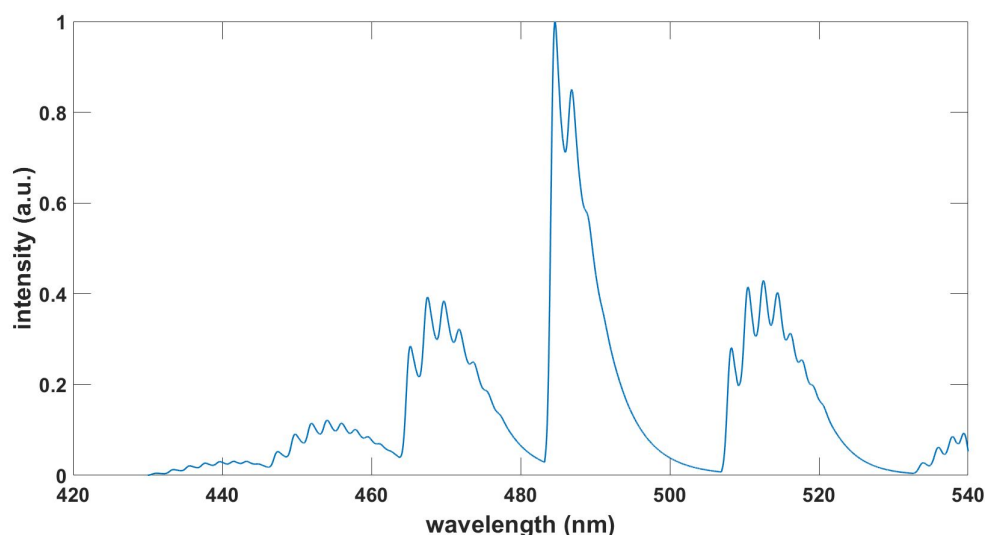


Figure 1. Computed AlO spectrum, $\Delta v = 0, \pm 1, \pm 2, +3$, $\delta\lambda = 1.0$ nm, $T = 3.33$ kK.

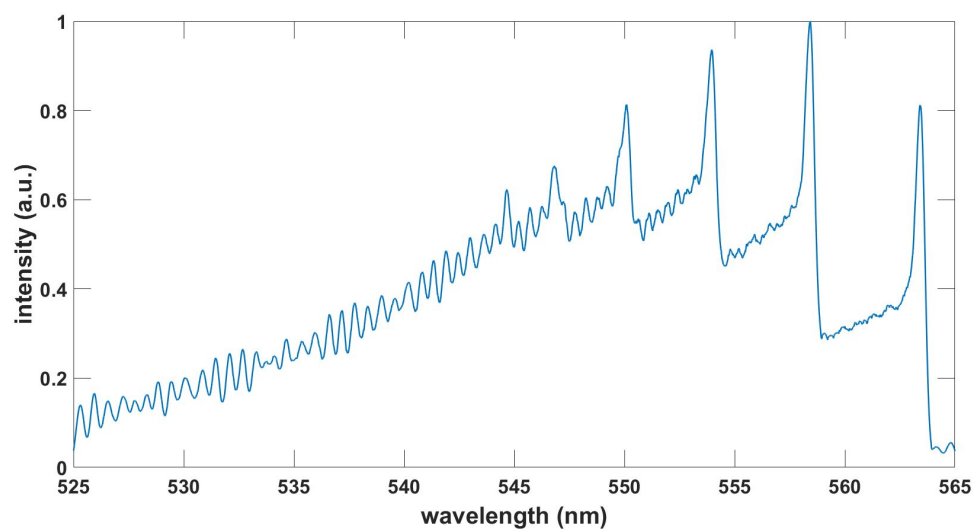


Figure 2. Computed C₂ Swan spectrum, $\Delta v = -1$, $\delta\lambda = 0.39$ nm, $T = 6.75$ kK.

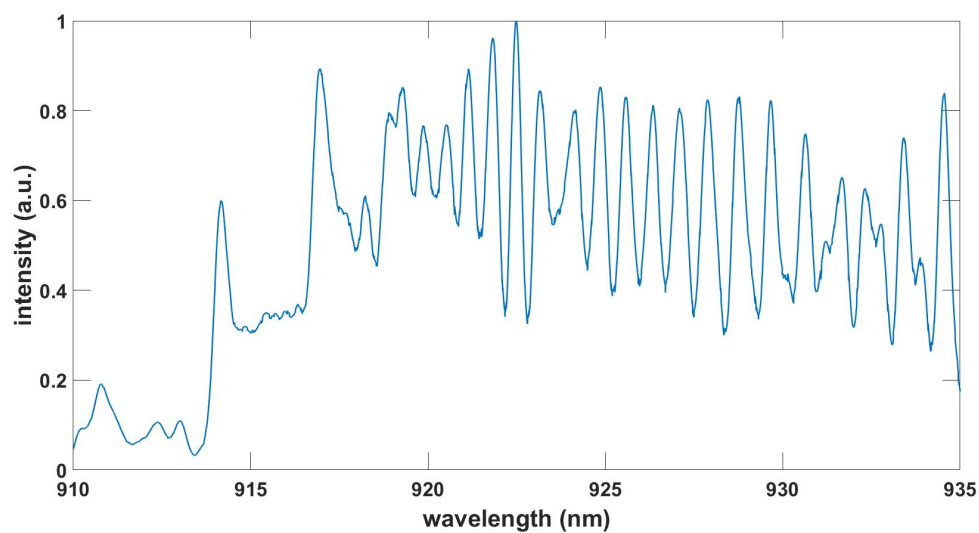


Figure 3. Computed CN red spectrum, $\Delta v = +1$, $\delta\lambda = 0.38$ nm, $T = 7.5$ kK.

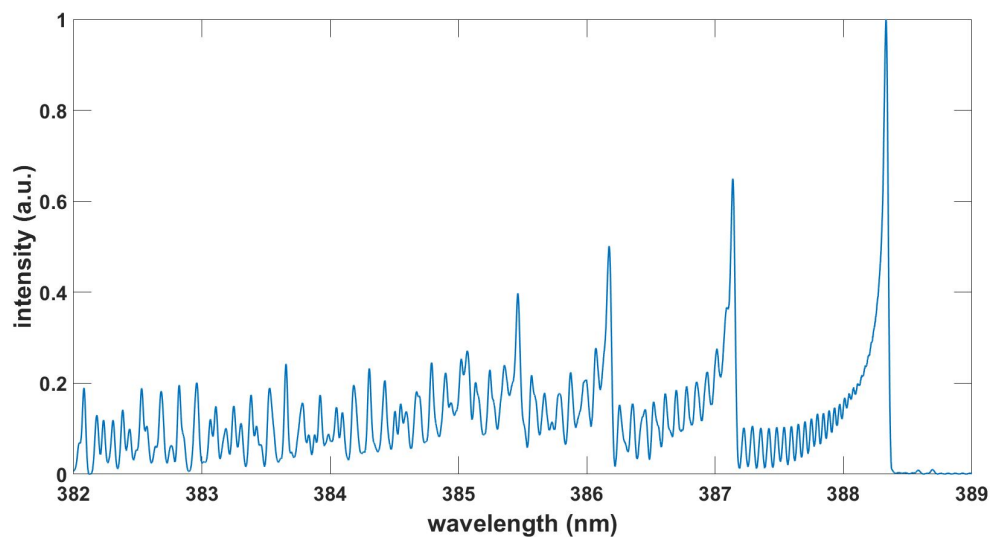


Figure 4. Computed CN violet spectrum, $\Delta v = 0$, $\delta\lambda = 0.030$ nm, $T = 7.94$ kK.

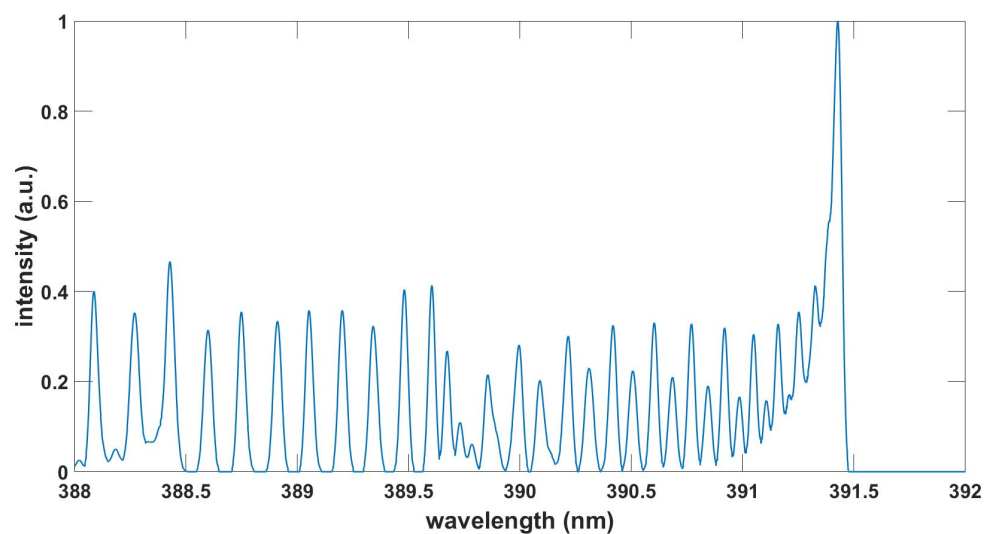


Figure 5. Computed N_2^+ spectrum, $\Delta v = 0$, $\delta\lambda = 0.035$ nm, $T = 5.1$ kK.

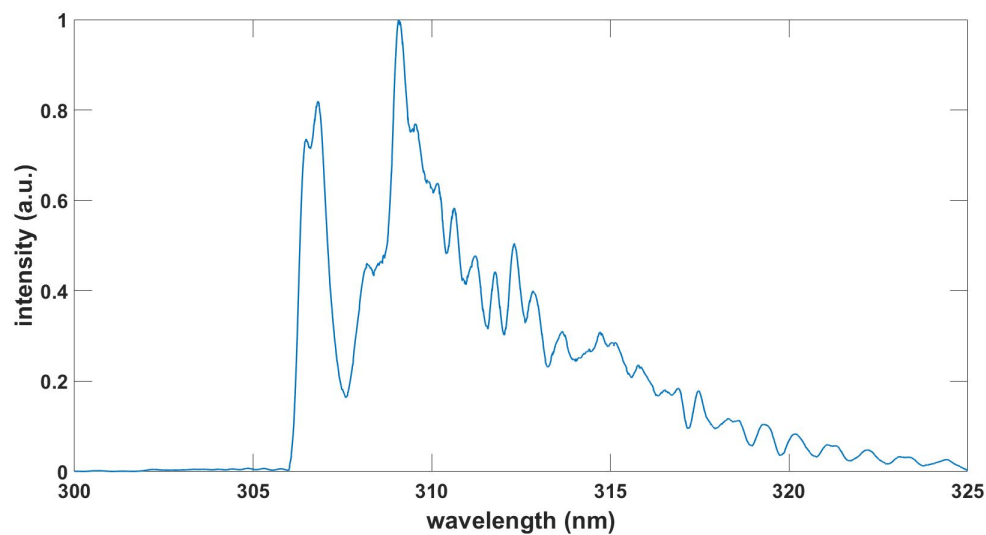


Figure 6. Computed OH spectrum, $\Delta v = 0$, $\delta\lambda = 0.35$ nm, $T = 3.39$ kK, see BESP.m script and Ref. [30].

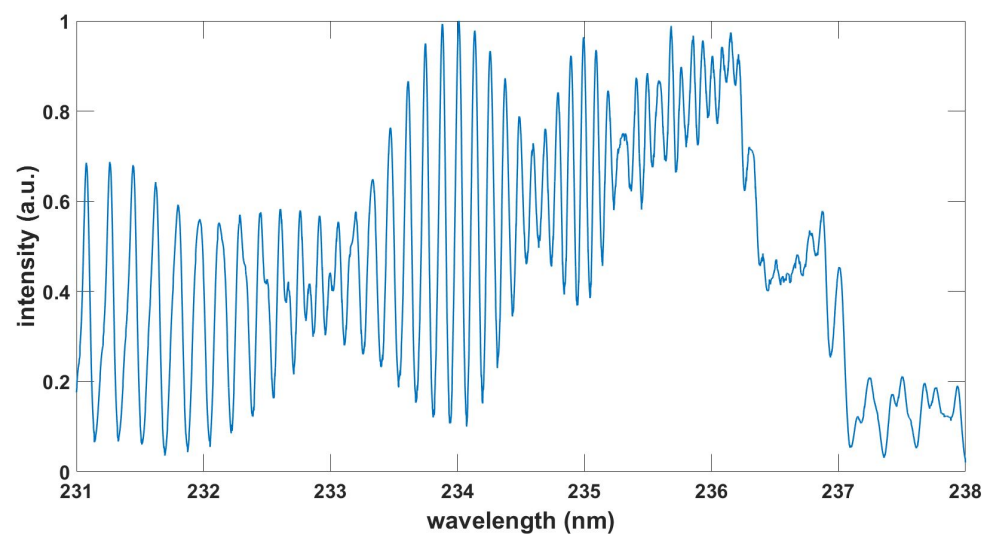


Figure 7. Computed NO gamma spectrum, $\Delta v = -1$, $\delta\lambda = 0.056$ nm, $T = 6.80$ kK.

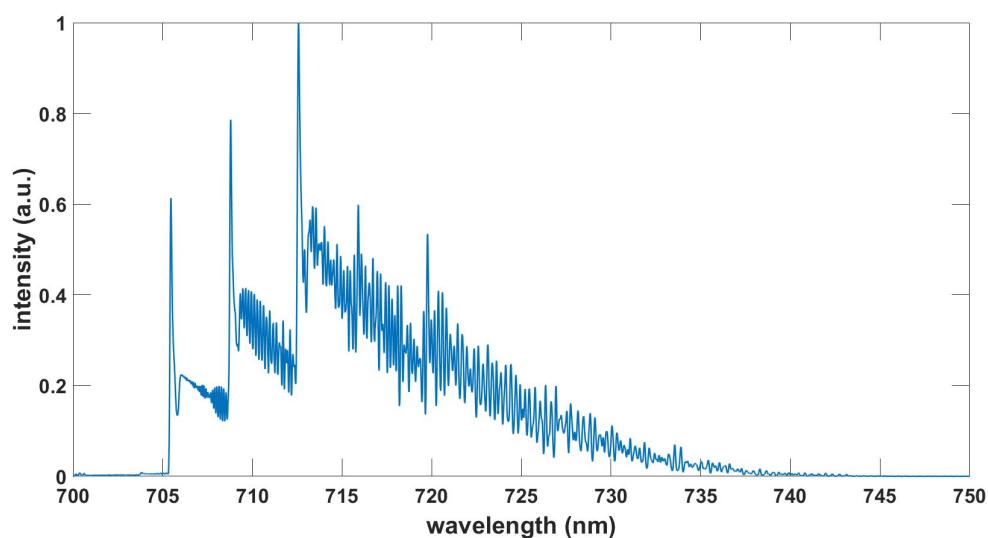


Figure 8. Computed TiO γ spectrum, $\Delta v = 0$, $\delta\lambda = 0.10$ nm, $T = 3.03$ kK.

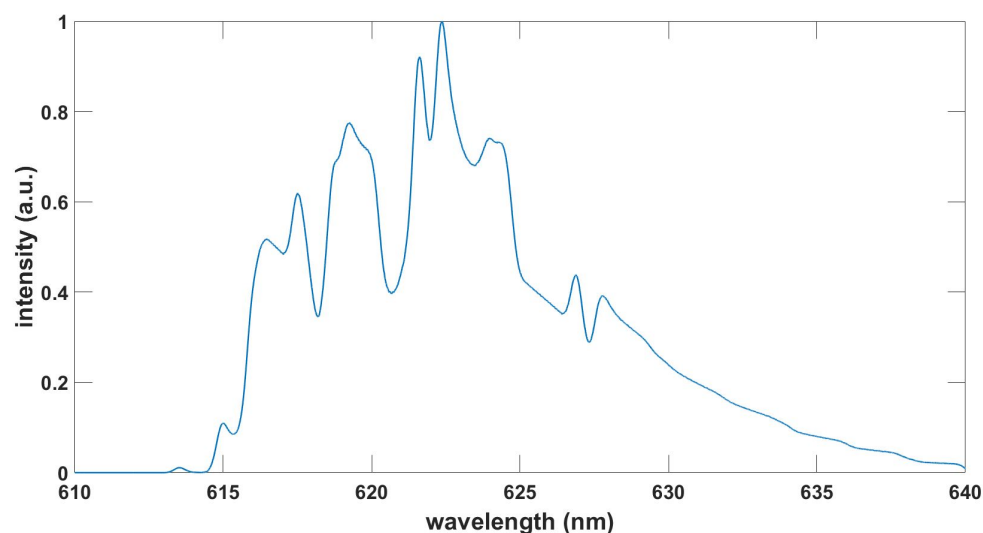


Figure 9. Computed TiO γ' spectrum, $\Delta v = 0$, $\delta\lambda = 0.40$ nm, $T = 3.6$ kK.

4. Discussion

The accurate prediction of line positions of diatomic molecules is important for the identification and of course for the fitting of measured data. The line positions are usually more accurate than the intensity values. The selected transitions for most of the communicated diatomic molecules, especially AlO, C₂ Swan, CN, and OH, have been extensively tested in the study of laser-induced optical breakdown. Comparisons of analysis of an experimental OH ultraviolet data record using the communicated OH table and the recent and updated ExoMol diatomic molecular databases reveal agreements of most wavelength positions, of the order of 10% variations of the line strengths, but better than 3% agreement in fitted temperature, spectral resolution and background. This bodes well for applications of expansive databases such as ExoMol in analytical laser-plasma research for the other diatomic molecules communicated in this work.

Supplementary Materials: The following supporting information can be down-loaded at: <https://www.mdpi.com/article/10.3390/foundations3010001/s1>. This supplement contains 9 diatomic line strength files plus 1 ExoMol-OH line strength file (see Appendix A), 1 example OH-experiment file, 2 MATLAB programs, and 2 graphical file2 that shows fitting of the OH-experiment with NMT_foundations_2.m - the program BESP_foundations_2.m computes theoretical spectra from the diatomic line strength files, and it also shows 1 graphical file.

Funding: This research received no specific external funding.

Institutional Review Board Statement: Not applicable.

Informed Consent Statement: Not applicable.

Data Availability Statement: Not applicable.

Acknowledgments: The authors acknowledges the support in part by the Center for Laser Applications at the University of Tennessee Space Institute.

Conflicts of Interest: The author declares no conflict of interest. The funders had no role in the design of the study; in the collection, analyses, or interpretation of data; in the writing of the manuscript, or in the decision to publish the results.

Abbreviations

The following abbreviations are used in this manuscript:

BESP	Boltzmann Equilibrium Spectral Program
AMO	Atomic, Molecular, Optical
AlO	Aluminum Monoxide
C ₂	Diatomic Carbon
CNr	Cyanide red system
CNv	Cyanide violet system
ExoMol	Molecular line lists for exoplanet and other hot atmospheres
FWHM	Full-Width at Half Maximum
HITEMP	High temperature molecular spectroscopic database
LIBS	Laser-Induced Breakdown Spectroscopy
LSF	Line-Strength file
NMT	Nelder–Mead Temperature
OH	Hydroxyl
N ₂ ⁺	singly ionized nitrogen
NO	Nitrogen Monoxide
PGOPHER	Program for simulating rotational, vibrational and electronic spectra
SATP	Standard Ambient Temperature and Pressure
TiO-AX	Titanium Monoxide γ band
TiO-BX	Titanium Monoxide γ' band
wIRE	Wiley interdisciplinary reviews

Appendix A

This Appendix communicates the NMT.m script for the fitting of recorded experimental data. Figure A1 shows the output in graphical form when using the data in the file OH-LSF.txt. The data file OH100micros.dat is included in the supplement. The fitting program also incorporates a slight, overall wavelength offset of $W_{\text{offset}} = -0.05$ nm for the data file OH100micros.dat. Measurement of laser-plasma emissions shows a background from other species as discussed in Ref. [39]. Fitting with the ExoMol [10] ¹⁶O¹H database [40–42] requires preparation of provided transition and state files to be consistent with the NMT.m input portion of the program. Figure A2 displays the results. The temperatures differ by 0.1 kK, spectral resolution by 0.01 nm and there is a slightly different linear background.

The HITEMP [11] database file 13_HITEMP2020.par for OH (57,019 lines) predicts a spectrum that is practically identical to the one from ExoMol (54,276 transitions, 1878 states) in the wavelength range of 305.17 nm to 321.83 nm for the experimental data OH100micros.dat. There are other OH databases that can be applied in the analysis of the OH emission spectra; for example, see LIFBASE [43] with associated OH transition probabilities [44]. LIFBASE shows data for molecules of interest in this work, namely OH (A-X), NO(A-X,B-X,C-X,D-X), CN(B-X) and N₂⁺(B-X).

Table A1 shows comparisons for the wavelength range of the communicated OH UV (A-X) data file OH100micros.dat. There are 328 extra lines in the ExoMol.dat file, with most

lines showing Einstein A coefficients that are larger than $1 \times 10^3 \text{ s}^{-1}$ and higher vibrational levels than those for OH-LSF.txt. Subsequent to correction of an overall term-value offset in the ExoMol OH data, T_{offset} , of $T_{\text{offset}} = 1809.4876$, the 512 transitions are labelled “equal” for transition wave numbers that differ by less than 0.5 cm^{-1} . It is noteworthy that 497 out of the 512 lines agree within 0.1 cm^{-1} .

Table A1. Comparison of ExoMol-OH.dat and OH-LSF.txt line strengths in the wavelength range from 305.17 nm to 321.83 nm in the experimental data OH100micro.dat.

Data File	Transition Lines	Equal Lines	Vibrational Levels
ExoMol.dat	856	512	0,1,2,3,4
OH-LSF.txt	528	512	0,1

The ExoMol database shows Einstein A coefficients that are converted to line strengths, S_{ul} , for electric dipole transitions [45], using (MKS units)

$$A_{ul} = \frac{16\pi^3}{3g_u h \epsilon_0 \lambda^3} (ea_0)^2 S_{ul}, \quad g_u = 2(2J_u + 1), \quad (\text{A1})$$

where A_{ul} denotes the Einstein A coefficient for a transition from an upper, u , to a lower, l , state, and h and ϵ_0 are Planck’s constant and vacuum permittivity, respectively. The elementary charge is e , the Bohr radius is a_0 , and S_{ul} is the transition strength. The line strength, S , that is used in the MATLAB scripts is expressed in traditional cgs units ($\text{stC}^2 \text{ cm}^2$, see Table 5). The wavelength of the transition is λ , g_u is the upper state degeneracy and J_u the total angular momentum of the upper state.

For the 512 lines with practically equal transition wave numbers, the ratios of ExoMol-OH.dat and OH-LSF.txt strengths show the mean value 1.093 with a standard deviation of 0.071. This line-strength variation may have several causes including differences in Hönl-London terms, Frank-Condon factors, and/or r-centroids. The fitted temperature indicates a 2.8% increase from 3.53 kK to 3.63 kK despite a mean 9.3% difference in line strengths. The NMT.m fitting script requires only relative intensities in the inference of temperature from measured spectra.

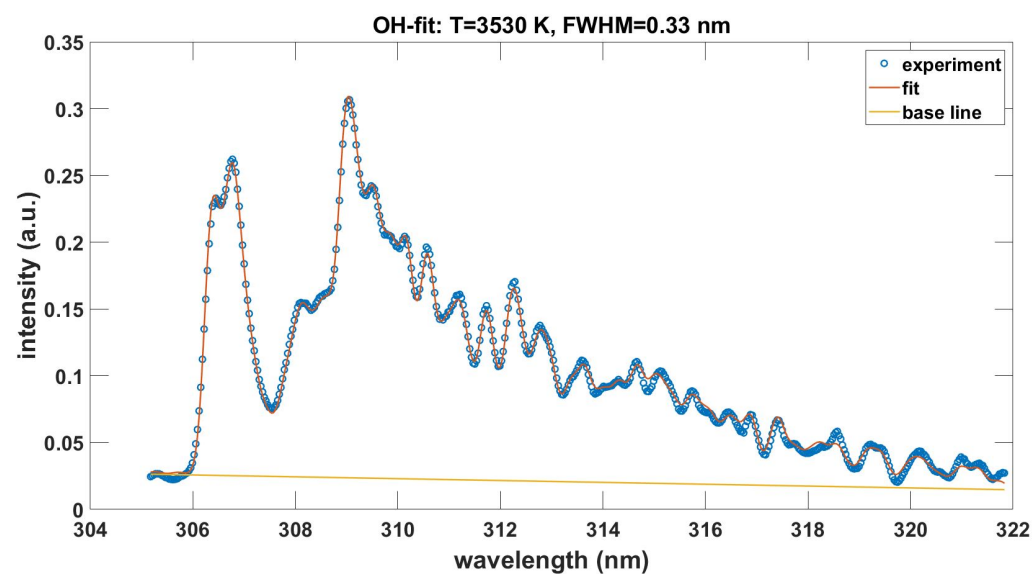


Figure A1. Measured and with OH-LSF.txt fitted OH emission spectra, $\Delta v = 0$, $\delta \lambda = 0.33 \text{ nm}$, $T = 3.53 \text{ kK}$.

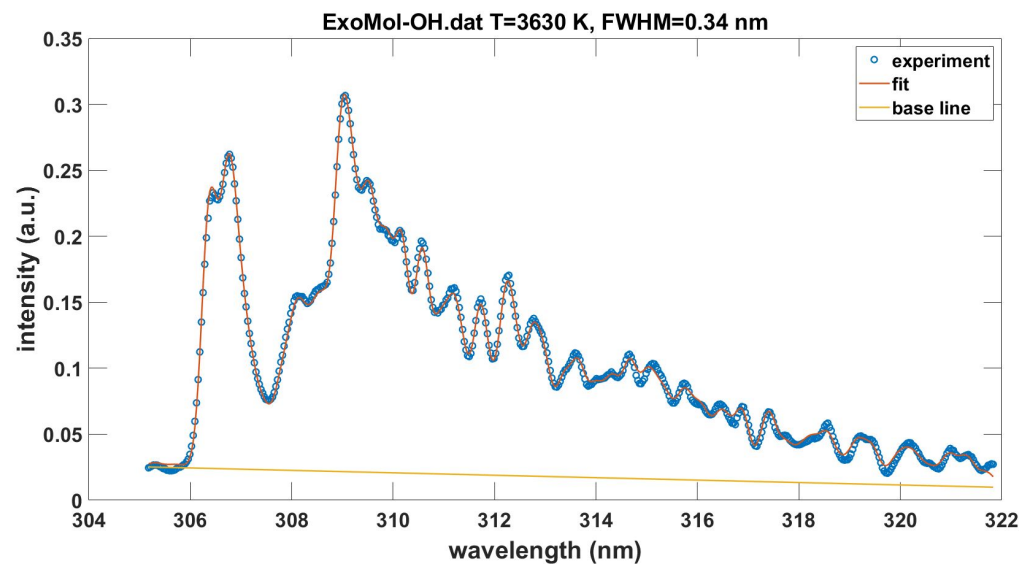


Figure A2. Measured and with ExoMol-OH.dat fitted OH emission spectra, $\Delta v = 0$, $\delta\lambda = 0.34$ nm, $T = 3.63$ kK.

```
% NMT.m
%
% Fits measured diatomic spectra using line strength data files constructed for selected transitions.
% The program is designed using a previous FORTRAN/Windows7 implementation including private communications
% with James O. Hornkohl and David M Surmick.
%
% inputs: WL_exp — experimental wavelengths (n x 1 array)
%         Dat    — experimental spectrum (n x 1 array)
%         FWHM   — measured spectral resolution, seed for varried FWHM or
%               fixed
%         T      — temperature seed for fitting
%         tol    — tolerance of Nelder-Mead fit
%         x      — name of line strength file for calculating theory spectra
%         FIT    — enter 1 for fitting linear offset and temperature
%               enter 2 for fitting linear offset, temperature, and FWHM
%
% outputs: profile — matrix containing experimental wavelengths, measured
%               spectrum, fitted spectrum, fitted baseline offset
%               (n x 4 matrix)
%         vals     — array containing fitted paramters (3x1 or 4x1 array),
%               temperature is always last entry
%
% sub-functions: FitSpec, FitSpec1, SynthSpec
%
% Example call: [I,v]=NMT(x,y1,0.15,3000,1e-8,'OH-LSF.txt',2);
%
% David M. Surmick, 04-28-2016, edited by Christian G Parigger 11-27-2022

function [profile,vals] = NMT (WL_exp,Dat,FWHM,T,tol,x,FIT)
tic % start code timer

% global variables
global bFac gFac WLk Tuk TuMin Sk n0 nSpec fwhm delWL temp wL_max;

% constants in MKS units (Boltzmann factor bfac in cgs units)
h=6.62606957e-34; c=2.99792458e8; kb=1.3806488e-23; bFac=(100*h*c)/kb; gFac=2*sqrt(log(2));

%load experimental data, here an OH spectrum 100 microsecond time delay in air breakdown.
xexp='OH100micros.dat';data=load(xexp);WL_exp=data(:,1);Dat=data(:,2);nSpec=length(Dat);

% input parameters
T=2000; FWHM=0.3; x='OH-LSF.txt'; temp=T; fwhm=FWHM; wL_min=min(WL_exp); wL_max=max(WL_exp); delWL=(wL_max-
wL_min)/(nSpec);

% read rprovided LSF file
ZZ=readtable(x); WN=ZZ.Var1; Tu=ZZ.Var2; S=ZZ.Var3;

% convert vacuum wavenumber to air wavelength: CGP 11-27-2022
```

```

% a0=2.72643e-4; a1=1.2288; a2=3.555e4; r=1+a0+(a1./(WN.*WN))+(a2./(WN.*WN.*WN.*WN));
k0=238.0185;k1=5792105;k2=57.362;k3=167917;WLOffset=0;r=(1+k1./(1e8*k0-(WN.*WN)))+k3./(1e8*k2-(WN.*WN));
WLOffset=0;if(xexp=='OH100micros.dat'); WLOffset=-0.05;end;WL=1.e7./(r.*WN)+WLOffset;

% get LSF table wavelengths in experimental range
A=find(WL>wL_min & WL<wL_max); WLk=WL(A);

% get Term Values and LineStrengths at WLk
Sk=S(A); Tuk=Tu(A); TuMin=min(Tuk);

% get expirmental wavelength positions that most closely matches line strength table wavelengths
n0=zeros(length(WLk),1); for i=1:length(WLk); [~,n0(i)]=min(abs(WL_exp-WLk(i))); end;

% normalize data
%Dat=Dat/max(Dat);

% Fitting with Nelder-Mead parameters including two cases options
tol=1.e-6; FIT=2; options=optimset('TolX',tol,'MaxIter',1e8,'MaxFunEvals',1e8);
switch FIT
case 1 % fit offset, temperature
    theta=ones(3,1);
    theta(3)=T; % temperature seed
    vals=fminsearch(@(x) FitSpec(x,WL_exp,Dat),theta,options);
    bkg=vals(1)+vals(2)*WL_exp; % calculate fitted offset
    [I,bkg1]=SynthSpec(WL_exp,vals(3),FWHM,Dat,bkg); % calculate fit
case 2 % fit offset, fwhm, temperature
    theta=ones(4,1);
    theta(3)=FWHM; % fwhm seed
    theta(4)=T; % temperature seed
    vals=fminsearch(@(x) FitSpec1(x,WL_exp,Dat),theta,options);
    bkg=vals(1)+vals(2)*WL_exp; % calculate fitted offset
    [I,bkg1]=SynthSpec(WL_exp,vals(4),vals(3),Dat,bkg); % calculate fit
end

% Visualize Fit
fname=regexprep(x,'-LSF.txt','_fit:');
figure
switch FIT
case 1
    plot(WL_exp,Dat,'o',WL_exp,I,WL_exp,bkg1,'LineWidth',1.5)
    legend('experiment','fit','base line')
    set(gca,'FontWeight','bold','FontSize',16,'TickLength',[0.02, 0.02]);
    val3=round(vals(3),3, 'significant')
    title([num2str(fname), 'T=',num2str(vals(3)),' K ,FWHM=',num2str(FWHM), 'nm'])
    xlabel('wavelength (nm)')
    ylabel('intensity (a.u.)')
case 2
    plot(WL_exp,Dat,'o',WL_exp,I,WL_exp,bkg1,'LineWidth',1.5)
    legend('experiment','fit','base line')
    set(gca,'FontWeight','bold','FontSize',20,'TickLength',[0.02, 0.02]);
    round(vals(4),3,'significant'); round(vals(3),2,'significant');
    val4=round(vals(4),3, 'significant'); val3=round(vals(3),2, 'significant');
    title([num2str(fname), ' T=',num2str(val4), ' K, FWHM=',num2str(val3), ' nm'])
    xlabel('wavelength (nm)','FontSize',24,'FontWeight','bold')
    ylabel('intensity (a.u.)','FontSize',24,'FontWeight','bold')
end

toc % end code timer

end % main function

% temperature, offset fit function
function [err] = FitSpec (p,WL_exp,Dat);
global fwhm;
bkg=p(1)+p(2)*WL_exp; [F,~]=SynthSpec(WL_exp,p(3),fwhm,Dat,bkg); c=F\Dat; z=F*c; err=norm(z-Dat);
end % fit spec

% temperature, fwhm, offset fit function
function [err] = FitSpec1 (p,WL_exp,Dat);
bkg=p(1)+p(2)*WL_exp; [F,~]=SynthSpec(WL_exp,p(4),p(3),Dat,bkg); c=F\Dat; z=F*c; err=norm(z-Dat);
end % fit spec 1

% calculate synthetic spectrum for fit
function [I1,bkg1] = SynthSpec (WL_exp,T,FWHM,Dat,bkg);
global bFac gFac WLk Tuk TuMin Sk n0 nSpec delWL wL_max;
FWHMk=(FWHM*WLk)/wL_max; % wavelength dependent FWHM

% Calculate Peak Intensities
peak=-4*log(WLk)+log(Sk)-(bFac/T)*(Tuk-TuMin); peak_k=exp(peak);

% calculate synthetic spectrum

```

```

I=zeros(nSpec,1); % initialize synthetic spectrum output
for i=1:length(WLk); deln=round(2.5*FWHMk(i)/delWL); nMin=n0(i)-deln;
    if nMin < 1; nMin=1; end;
    nMax=n0(i)+deln;
    if nMax > nSpec; nMax=nSpec; end;
    for j=nMin:nMax; u=abs(gFac*(WLk(i)-WL_exp(j))/FWHMk(i)); I(j)=I(j)+peak_k(i)*exp(-u*u); end;
end % synthetic spectrum loop

% normalize data to measured spectrum
I=I/max(I); I=I+bkg; sxy=sum(Dat.*I); sy=sum(I.*I); nf= sxy/syy; I1=I*nf; bkg1=bkg*nf;
end % SynthSpec

```

References

- Kunze, H.-J. *Introduction to Plasma Spectroscopy*; Springer: Berlin/Heidelberg, Germany, 2009.
- Fujimoto, T. *Plasma Spectroscopy*; Clarendon Press: Oxford, UK, 2004.
- Ochkin, V.N. *Spectroscopy of Low Temperature Plasma*; Wiley-VCH: Weinheim, Germany, 2009.
- Omenetto, N. (Ed.) *Analytical Laser Spectroscopy*; John Wiley & Sons: New York, NY, USA, 1979.
- Demtröder, W. *Laser Spectroscopy 1: Basic Principles*, 5th ed.; Springer: Heidelberg, Germany, 2014.
- Demtröder, W. *Laser Spectroscopy 2: Experimental Techniques*, 5th ed.; Springer: Heidelberg, Germany, 2015.
- Hertel, I.V.; Schulz, C.-P. *Atoms, Molecules and Optical Physics 1, Atoms and Spectroscopy*; Springer: Heidelberg, Germany, 2015.
- Hertel, I.V.; Schulz, C.-P. *Atoms, Molecules and Optical Physics 2, Molecules and Photons—Spectroscopy and Collisions*; Springer: Heidelberg, Germany, 2015.
- McKemmish, L.K. Molecular diatomic spectroscopy data. *WIREs Comput. Mol. Sci.* **2021**, *11*, e1520. [[CrossRef](#)]
- Tennyson, J.; Yurchenko, S.N.; Al-Refaie, A.F.; Clark, V.H.J.; Chubb, K.L.; Conway, E.K.; Dewan, A.; Gorman, M.N.; Hill, C.; Lynas-Gray, A.E.; et al. The 2020 release of the ExoMol database: Molecular line lists for exoplanet and other hot atmospheres. *J. Quant. Spectrosc. Radiat. Transf.* **2020**, *255*, 107228. [[CrossRef](#)]
- Rothman, L.S.; Gordon, I.E.; Barber, R.J.; Dothe, H.; Gamache, R.R.; Goldman, A.; Perevalov, V.I.; Tashkun, S.A.; Tennyson, J. HITEMP, the high-temperature molecular spectroscopic database. *J. Quant. Spectrosc. Radiat. Transf.* **2010**, *111*, 2139–2150. [[CrossRef](#)]
- Western, C.M. PGOPHER, A Program for Simulating Rotational, Vibrational and Electronic Spectra. *J. Quant. Spectrosc. Radiat. Transf.* **2017**, *186*, 221–242. [[CrossRef](#)]
- Miziolek, A.W.; Palleschi, V.; Schechter, I. (Eds.) *Laser Induced Breakdown Spectroscopy (LIBS): Fundamentals and Applications*; Cambridge Univ. Press: New York, NY, USA, 2006.
- Singh, J.P.; Thakur, S.N. (Eds.) *Laser-Induced Breakdown Spectroscopy*, 2nd ed.; Elsevier: Amsterdam, The Netherlands, 2020.
- De Giacomo, A.; Hermann, J. Laser-induced plasma emission: From atomic to molecular spectra. *J. Phys. D Appl. Phys.* **2017**, *50*, 183002. [[CrossRef](#)]
- Parigger, C.G. Laser-induced breakdown in gases: Experiments and simulation. In *Laser Induced Breakdown Spectroscopy (LIBS): Fundamentals and Applications*; Miziolek, A.W., Palleschi, V., Schechter, I., Eds.; Cambridge Univ. Press: New York, NY, USA, 2006; Chapter 4; pp. 171–193.
- Parigger, C.G.; Surmick, D.M.; Helstern, C.M.; Gautam, G.; Bol'shakov, A.A.; Russo, R. Molecular Laser-Induced Breakdown Spectroscopy. In *Laser Induced Breakdown Spectroscopy*, 2nd ed.; Singh, J.P., Thakur, S.N., Eds.; Elsevier: Amsterdam, The Netherlands, 2020; Chapter 7; pp. 167–212.
- Parigger, C.G.; Helstern, C.M.; Jordan, B.S.; Surmick, D.M.; Splinter, R. Laser-Plasma Spatiotemporal Cyanide Spectroscopy and Applications. *Molecules* **2020**, *25*, 615. [[CrossRef](#)] [[PubMed](#)]
- Parigger, C.G.; Helstern, C.M.; Jordan, B.S.; Surmick, D.M.; Splinter, R. Laser-Plasma Spectroscopy of Hydroxyl with Applications. *Molecules* **2020**, *25*, 988. [[CrossRef](#)]
- Parigger, C.G. Review of spatiotemporal analysis of laser-induced plasma in gases. *Spectrochim. Acta Part B At. Spectrosc.* **2021**, *179*, 106122. [[CrossRef](#)]
- Parigger, C.G.; Woods, A.C.; Surmick, D.M.; Gautam, G.; Witte, M.J.; Hornkohl, J.O. Computation of diatomic molecular spectra for selected transitions of aluminum monoxide, cyanide, diatomic carbon, and titanium monoxide. *Spectrochim. Acta Part B At. Spectrosc.* **2015**, *107*, 132–138. [[CrossRef](#)]
- Parigger, C.G.; Hornkohl, J.O. *Quantum Mechanics of the Diatomic Molecule with Applications*; IOP Publishing: Bristol, UK, 2020.
- Hornkohl, J.O.; Nemes, L.; Parigger, C.G. Spectroscopy of Carbon Containing Diatomic Molecules. In *Spectroscopy, Dynamics and Molecular Theory of Carbon Plasmas and Vapors: Advances in the Understanding of the Most Complex High-Temperature Elemental System*; Nemes, L., Irle, S., Eds.; World Scientific: Singapore, 2011; Chapter 4; pp. 113–165.
- Surmick, D.M.; Hornkohl, J.O. (The University of Tennessee, University of Tennessee Space Institute, Tullahoma, TN, USA). Personal communication, 2016.
- MATLAB Release R2022a Update 5; The MathWorks, Inc.: Natick, MA, USA, 2022.

26. Parigger, C.G.; Woods, A.C.; Witte, M.J.; Swafford, L.D.; Surmick, D.M. Measurement and analysis of atomic hydrogen and diatomic molecular AlO, C₂, CN, and TiO spectra following laser-induced optical breakdown. *J. Vis. Exp.* **2014**, *84*, e51250.
27. Barrell, H.; Sears, J.E. The Refraction and Dispersion of Air for the Visible Spectrum. *Philos. Trans. R. Soc. Lond.* **1939**, *238*, 1–64.
28. Ciddor, P.E. Refractive index of air: New equations for the visible and near infrared. *Appl. Opt.* **1996**, *35*, 1567–1573. [[CrossRef](#)] [[PubMed](#)]
29. Corney, A. *Atomic and Laser Spectroscopy*; Clarendon Press: Oxford, UK, 1977.
30. Parigger, C.G. Hydroxyl Spectroscopy of Laboratory Air Laser-Ignition. *Foundations* **2022**, *2*, 934–948. [[CrossRef](#)]
31. Dors, I.G.; Parigger, C.; Lewis, J.W.L. Spectroscopic temperature determination of aluminum monoxide in laser ablation with 266-nm radiation. *Opt. Lett.* **1998**, *23*, 1778–1780. [[CrossRef](#)]
32. Parigger, C.; Plemmons, D.H.; Hornkohl, J.O.; Lewis, J.W.L. Spectroscopic Temperature Measurements in a Decaying Laser-Induced Plasma Using the C₂ Swan System. *J. Quant. Spectrosc. Radiat. Transf.* **1994**, *52*, 707–711. [[CrossRef](#)]
33. Trautner, S.; Jasik, J.; Parigger, C.G.; Pedarnig, J.D.; Spendelhofer, W.; Lackner, J.; Veis, P.; Heitz, J. Laser-induced breakdown spectroscopy of polymer materials based on evaluation of molecular emission bands. *Spectrochim. Acta Part A Mol. Biomol. Spectrosc.* **2017**, *174*, 331–338. [[CrossRef](#)]
34. Hornkohl, J.O.; Parigger, C.; Lewis, J.W.L. Temperature Measurements from CN Spectra in a Laser-Induced Plasma. *J. Quant. Spectrosc. Radiat. Transf.* **1991**, *46*, 405–411. [[CrossRef](#)]
35. Parigger, C.; Plemmons, D.H.; Hornkohl, J.O.; Lewsi, J.W.L. Temperature measurements from first-negative N₂⁺ spectra produced by laser-induced multiphoton ionization and optical breakdown of nitrogen. *Appl. Opt.* **1995**, *34*, 3331–3335. [[CrossRef](#)] [[PubMed](#)]
36. Hornkohl, J.O.; Fleischmann, J.P.; Surmick, D.M.; Witte, M.J.; Swaffor, L.D.; Woods, A.C.; Parigger, C.G. Emission spectroscopy of nitric oxide in laser-induced plasma. *J. Phys. Conf. Ser.* **2014**, *548*, 12040. [[CrossRef](#)]
37. Parigger, C.G.; Woods, A.C.; Keszler, A.; Nemes, L.; Hornkohl, J.O. Titanium monoxide spectroscopy following laser-induced optical breakdown. *AIP Conf. Proc.* **2012**, *1464*, 628–639.
38. Woods, A.C.; Parigger, C.G.; Hornkohl, J.O. Measurement and analysis of titanium monoxide spectra in laser-induced plasma. *Opt. Lett.* **2012**, *37*, 5139–5141. [[CrossRef](#)] [[PubMed](#)]
39. Parigger, C.G.; Guan, G.; Hornkohl, J.O. Measurement and analysis of OH emission spectra following laser-induced optical breakdown in air. *Appl. Opt.* **2003**, *42*, 5986–5991. [[CrossRef](#)] [[PubMed](#)]
40. Brooke, J.S.A.; Bernath, P.F.; Western, C.M.; Sneden, C.; Afşar, M.; Li, G.; Gordon, I.E. Line strengths of rovibrational and rotational transitions in the X²Π ground state of OH. *J. Quant. Spectrosc. Radiat. Transf.* **2016**, *138*, 142–157. [[CrossRef](#)]
41. Yousefi, M.; Bernath, P.F.; Hodges, J.; Masseron, T. A new line list for the A²Σ – X²Π electronic transition of OH. *J. Quant. Spectrosc. Radiat. Transf.* **2018**, *217*, 416–424. [[CrossRef](#)]
42. Bernath, P.F. MoLLIST: Molecular Line Lists, Intensities and Spectra. *J. Quant. Spectrosc. Radiat. Transf.* **2020**, *240*, 106687. [[CrossRef](#)]
43. Luque, J.; Crosley, D.R. LIFBASE: Database and Spectral Simulation for Diatomic Molecules. 2021. Available online: <https://www.sri.com/platform/lifbase-spectroscopy-tool> (accessed on 25 November 2019).
44. Luque, J.; Crosley, D.R. Transition probabilities in the A²Σ⁺ – X²Π_i electronic system of OH. *J. Chem. Phys.* **1998**, *109*, 439–448. [[CrossRef](#)]
45. Tatum, J. *Stellar Atmospheres*; Open Education Resource LibreTexts Project: LibreTexts Physics, Shared under CC BY-NC 4.0 Licence; Last Updated March 5; University of Victoria: Victoria, BC, Canada, 2022.

Disclaimer/Publisher’s Note: The statements, opinions and data contained in all publications are solely those of the individual author(s) and contributor(s) and not of MDPI and/or the editor(s). MDPI and/or the editor(s) disclaim responsibility for any injury to people or property resulting from any ideas, methods, instructions or products referred to in the content.